

Testing the interaction of dark energy to dark matter through the analysis of virial relaxation of clusters Abell Clusters A586 and A1689 using realistic density profiles

Orfeu Bertolami · Francisco. Gil Pedro ·
Morgan Le Delliou

Received: date / Accepted: date

Abstract Interaction between dark energy and dark matter is probed through deviation from the virial equilibrium for two relaxed clusters: A586 and A1689. The evaluation of the virial equilibrium is performed using realistic density profiles. The virial ratios found for the more realistic density profiles are consistent with the absence of interaction.

Keywords Cosmology · Gravitation · Dark Matter · Equivalence Principle · Field-theory

PACS 98.80.-k · 98.80.Cq

1 Introduction

Searching for evidence and possible strategies for detection of dark energy and dark matter are among the most pressing issues of contemporary physics. Dark energy (DE) and dark matter (DM) are the fundamental building blocks of the

O. Bertolami

Departamento de Física e Astronomia, Faculdade de Ciências da Universidade do Porto
Rua do Campo Alegre 687, 4169-007 Porto, Portugal

E-mail: orfeu.bertolami@fc.up.pt fgpedro@fisica.ist.utl.pt

O.B. Also at: Instituto de Plasmas e Fusão Nuclear, Instituto Superior Técnico, Avenida
Rovisco Pais 1, 1049-001 Lisboa, Portugal

F. Gil Pedro

Rudolf Peierls Centre for Theoretical Physics

1 Keble Road Oxford OX1 3NP, UK

E-mail: f.pedro1@physics.ox.ac.uk

M. Le Delliou

Instituto de Física Teórica UAM/CSIC, Facultad de Ciencias, C-XI, Universidad Autónoma
de Madrid, Cantoblanco, 28049 Madrid SPAIN E-mail: Morgan.LeDelliou@uam.es

Also at: Centro de de Astronomia e Astrofísica da Universidade de Lisboa, Faculdade de
Ciências da Universidade de Lisboa Edifício C8, Campo Grande P-1749-016 LISBOA Por-
tugal

cosmological standard model based on general relativity. If on one hand, the interaction of the dark sector with the standard model such as neutrinos [1] and the Higgs field [2] lead to well defined experimental implications, such as for instance, a possible deviation from the Rutherford-Soddy radiative decay law [4] (see eg. Ref. [5] for general discussions), on another hand, interaction within the dark sector itself should not be excluded. Indeed, a recent study [6] suggests that a putative interaction might also be detectable using for instance gamma-ray bursts. The interaction between dark energy and dark matter can be introduced either by ad hoc arguments [7] or because dark energy and dark matter are unified in the context of some framework [8–10]. Of course it is quite relevant to search for observational evidence of this interaction.

In a previous work [11] we have analysed the effect of the interaction between dark energy and dark matter on the virial equilibrium of clusters. Our method is based on the generalisation of the Layzer-Irvine equation, the cosmic virial theorem equation, which was then applied to the Abell cluster A586. This cluster was chosen given that it is presumably in equilibrium and has not undergone interactions for quite a long time [12]. We have also argued that, based on the analysis of the bias parameter, that the dark sector interactions do signal a possible violation of the Equivalence Principle at cosmological scale [11, 13]. This proposal has been extended for other clusters in Refs. [14], and as in our A586 analysis, evidence for DE-DM interaction was encountered.

In this work we reexamine the cluster A586 and extend our analysis to the Abell cluster A1689 considering that mass distribution within the cluster is not constant. The additional cluster A1689 is chosen as it shares with A586 the feature of showing a negligible amount of mergers, as inferred from its low X-ray substructure [15]. We consider four distinct density profiles: Navarro, Frenk and White (NFW) profile [16], isothermal sphere (ISO) profile [17–22], Moore’s (M) profile [23] and Einasto profile [24–26]. We also obtain results for up to four different techniques of evaluating the velocity dispersion σ_v of the haloes. We argue that the most relevant technique for determination of the velocity dispersion is through the X-ray temperature. Our analysis reveals that the use of more realistic mass profiles brings the virial ratio close to its canonical value in the absence of interaction.

This work is organized as follows: in section 2 we describe the techniques used for fitting the data with the various density profiles; section 3 presents our analysis of the virial ratios for the previously used cluster A586; section 4 considers the A1689 cluster; in section 5 we interpret our results in terms of DE-DM interaction. Finally, in section 6 we present our conclusions.

2 Computations of the Virial ratio for a given density profile

In this section we present our method and summarise the results of applying realistic density profiles to estimate the interaction between DE and DM in relaxed systems as discussed in Refs. [11,13]. We will focus on two relaxed galaxy clusters: A586, which was already analysed in Ref. [11] with a top-hat density profile, and A1689.

We start by defining the basic quantities and deriving the necessary relations between them. In particular we focus on obtaining various density profile fits for the haloes, and using the photometric coordinates of the galaxies, we compute the average distance between a galaxy and the centre of the cluster, $\langle R \rangle$, at which point we are in condition to evaluate the various density profiles parameters and the corresponding errors for the cluster A586. For the cluster A1689, we use weak lensing surface density data. To compute the virial ratio ρ_K/ρ_W we must also find the velocity dispersion σ_v . From Refs. [12,28,27,29] we obtain the weak lensing and photometric data necessary to compute the different density profiles as well as values for σ_v , as given by different methods; note that we approximate the velocity dispersion by its average value therefore considering it to be constant over the cluster ; we can then compute the ratio of kinetic energy to potential energy using different data sources (see Table 1 for A586 and Table 3 for A1689).

In Ref. [11] we have used the simplest approach of a Top-Hat density profile and used the velocity dispersion estimated from weak lensing measurements. For the purpose of comparison, we present in Table 2 the outputs of such profile with the same velocity dispersion as for the other more realistic profiles. Although that analysis allows for claiming detection [11], a more accurate estimate of the density leads to an underestimation of the potential energy by placing more mass far from the centre than a realistic decreasing profile. This implies an overestimate of the magnitude of the virial ratio, as can be seen for central values in Table 2. This should be corrected with the use of more realistic density profiles.

It is important to stress that the methods used vary slightly for the two clusters we are studying here. For the A586 we proceed in the same spirit as in Ref. [11], estimating the density and shape parameters for the several density profiles from total 3D mass and galaxy coordinates. On the other hand, for the A1689 cluster we fit directly the profiles to the 2D surface density obtained from lensing measurements [28].

2.1 NFW profile

Given its prominence in discussions about the density profile emerging from realistic N-body simulations in the context of the Λ CDM model, the NFW

density profile [16] will be used. It reads

$$\rho(r) = \frac{\rho_0}{\frac{r}{r_0} \left(1 + \frac{r}{r_0}\right)^2}, \quad (1)$$

where ρ_0 and r_0 are the density and shape parameters respectively. Note that since ρ only depends on r , spherical symmetry is built into these computations from the very start.

In the analysis of the cluster A1689, the 2D surface density from lensing measurements is used to perform a fit in order to obtain the estimates for ρ_0 and r_0 . For the cluster A586 we proceed by computing the mass by integrating Eq. (1) over the volume:

$$M \equiv 4\pi \int_0^R \frac{\rho_0 r^2}{\frac{r}{r_0} \left(1 + \frac{r}{r_0}\right)^2} dr = 4\pi r_0^3 \rho_0 \left[\ln \left(1 + \frac{R}{r_0}\right) - \frac{R}{R+r_0} \right]. \quad (2)$$

The mean radius $\langle R \rangle$ can then be defined with

$$M \langle R \rangle \equiv 4\pi \int_0^R \frac{\rho_0 r^3}{\frac{r}{r_0} \left(1 + \frac{r}{r_0}\right)^2} dr = 4\pi r_0^4 \rho_0 \left[\frac{R}{r_0} - 2 \ln \left(1 + \frac{R}{r_0}\right) + \frac{R}{R+r_0} \right], \quad (3)$$

which after considering Eq. (2) can be written as follows:

$$\langle R \rangle = r_0 \frac{\left[\frac{R}{r_0} - 2 \ln \left(1 + \frac{R}{r_0}\right) + \frac{R}{R+r_0} \right]}{\left[\ln \left(1 + \frac{R}{r_0}\right) - \frac{R}{R+r_0} \right]}. \quad (4)$$

We can then get the shape parameter r_0 for A586 by numerically inverting $\langle R \rangle$. We then use it to define the NFW density parameter ρ_0 from the observed mass M contained within the radius R by inverting Eq. (2):

$$\rho_0 = \frac{M}{4\pi r_0^3 \left[\ln \left(1 + \frac{R}{r_0}\right) - \frac{R}{R+r_0} \right]}. \quad (5)$$

The kinetic energy density is defined in terms of the average velocity dispersion, σ_v , to be

$$\rho_K = \frac{1}{2} \frac{3}{V} \int \rho \sigma_v^2 dV = \frac{9}{2} \frac{r_0^3}{R^3} \rho_0 \int_0^R \frac{r}{[r+r_0]^2} \sigma_v^2 dr. \quad (6)$$

Assuming a constant average velocity dispersion, it reads

$$\rho_K = \frac{1}{2} \frac{M}{V} 3\sigma_v^2 = \frac{9}{2} \frac{r_0^3}{R^3} \rho_0 \left[\ln \left(1 + \frac{R}{r_0}\right) - \frac{R}{R+r_0} \right] \sigma_v^2 = \frac{9}{8\pi} \frac{M}{R^3} \sigma_v^2, \quad (7)$$

as used in Ref. [11].

The potential energy is given by

$$\rho_W = -\frac{4\pi}{4\pi R^3/3} \int_0^R \frac{\rho(r)GM(r)}{r} r^2 dr \quad (8)$$

$$= -\frac{3GM^2}{4\pi R^3 r_0} \frac{\left[\left(1 + \frac{R}{r_0}\right) \left\{ \frac{1}{2} \left(1 + \frac{R}{r_0}\right) - \ln \left(1 + \frac{R}{r_0}\right) \right\} - \frac{1}{2} \right]}{\left[\left(1 + \frac{R}{r_0}\right) \ln \left(1 + \frac{R}{r_0}\right) - \frac{R}{r_0} \right]^2}. \quad (9)$$

As discussed in Ref. [11], the existence of interaction between DE and DM is estimated by comparing the ratio ρ_K/ρ_W with the expected $-1/2$ value arising from the virial theorem. Taking the ratio of Eqs. (7) and (9) we find:

$$\frac{\rho_K}{\rho_W} = -\frac{\frac{3}{2} \frac{r_0}{GM} \sigma_v^2 \left[\left(1 + \frac{R}{r_0}\right) \ln \left(1 + \frac{R}{r_0}\right) - \frac{R}{r_0} \right]^2}{\left[\left(1 + \frac{R}{r_0}\right) \left\{ \frac{1}{2} \left(1 + \frac{R}{r_0}\right) - \ln \left(1 + \frac{R}{r_0}\right) \right\} - \frac{1}{2} \right]}. \quad (10)$$

Throughout our analysis, the errors of the ratios are computed according to the following equation:

$$\Delta \left(\frac{\rho_K}{\rho_W}(\{o_i\}) \right) = \sqrt{\sum_{p_i \in \{o_i\}} \left(\frac{\partial \rho_K/\rho_W}{\partial p_i} \Delta(p_i) \right)^2}, \quad (11)$$

where $\{o_i\}$ are the parameters carrying measurement errors and are defined for each cluster as $\{o_i\} = \{\sigma_v, M\}$ for A586 and as $\{o_i\} = \{\sigma_v, r_0, \rho_0\}$ for A1689.

2.2 Isothermal profile

Introduced first as the natural outcome of spherically symmetric DM self-gravitating infall [17–22], the isothermal density profile is simpler than the NFW one:

$$\rho = \frac{\rho_0}{\left(\frac{r}{r_0}\right)^2}. \quad (12)$$

Here the fiducial radius r_0 and density ρ_0 , or mass $M_0 = 4\pi/3\rho_0 r_0^3$, are arbitrary as the profile is self-similar: there is no characteristic scale, so we can chose the mass and total radius of the halo as the fiducial values,

$$M_0 = M, \quad (13)$$

$$r_0 = R. \quad (14)$$

The mass is found by integrating Eq. (12) over the volume:

$$M \equiv 4\pi \int_0^R \frac{\rho_0 r^2}{\left(\frac{r}{r_0}\right)^2} dr = 4\pi r_0^2 R \rho_0 = M_0 \frac{R}{r_0}. \quad (15)$$

The mean radius $\langle R \rangle$ can then be defined with

$$M \langle R \rangle \equiv 4\pi \int_0^R \frac{\rho_0 r^3}{\left(\frac{r}{r_0}\right)^2} dr = 2\pi r_0^2 \rho_0 R^2, \quad (16)$$

which after considering Eq. (15) can be written as follows:

$$\langle R \rangle = \frac{R}{2}. \quad (17)$$

The new kinetic energy density is now defined to be

$$\rho_K = \frac{1}{2} \frac{3}{V} \int \rho \sigma_v^2 dV = \frac{9}{2} \frac{r_0^2}{R^3} \rho_0 \int_0^R \sigma_v^2 dr = \frac{9}{8\pi} \frac{M_0}{R^3 r_0} \int_0^R \sigma_v^2 dr. \quad (18)$$

Assuming a constant average velocity dispersion, it reads

$$\rho_K = \frac{1}{2} \frac{M}{V} 3\sigma_v^2 = \frac{9}{8\pi} \frac{M_0}{R^3 r_0} R \sigma_v^2 = \frac{9}{8\pi} \frac{M}{R^3} \sigma_v^2, \quad (19)$$

again as in Ref. [11].

The potential energy is given by

$$\rho_W = -\frac{4\pi}{4\pi R^3/3} \int_0^R \frac{\rho(r)GM(r)}{r} r^2 dr = -\frac{3GM_0^2}{4\pi R^2 r_0^2} = -\frac{3GM^2}{4\pi R^4}. \quad (20)$$

Taking the ratio of Eqs. (19) and (20) we find:

$$\frac{\rho_K}{\rho_W} = -\frac{3}{2} \frac{r_0}{GM_0} \sigma_v^2 = -\frac{3}{2} \frac{R}{GM} \sigma_v^2. \quad (21)$$

2.3 Moore's profile

We consider now the Moore density profile that also arises as a suitable dark halo profile from N-body simulations [23]. It is believed to be quite accurate to describe galaxy size halo formation [30]:

$$\rho = \frac{\rho_0}{\left(\frac{r}{r_0}\right)^{\frac{3}{2}} \left[1 + \left(\frac{r}{r_0}\right)^{\frac{3}{2}}\right]}, \quad (22)$$

where ρ_0 and r_0 are the new mass density and shape parameters, respectively. The mass is found by integrating Eq. (22) over the volume:

$$M = 4\pi \rho_0 \int_0^R \frac{r^2}{\left(\frac{r}{r_0}\right)^{\frac{3}{2}} \left[1 + \left(\frac{r}{r_0}\right)^{\frac{3}{2}}\right]} dr = \frac{8\pi}{3} r_0^3 \rho_0 \ln \left(1 + \left(\frac{R}{r_0}\right)^{\frac{3}{2}}\right). \quad (23)$$

The mean radius $\langle R \rangle$ can then be defined with

$$M \langle R \rangle = 4\pi r_0^3 \rho_0 \int_0^R \frac{\left(\frac{r}{r_0}\right)^{\frac{3}{2}}}{1 + \left(\frac{r}{r_0}\right)^{\frac{3}{2}}} dr, \quad (24)$$

and considering Eq. (23), it can be written as:

$$\langle R \rangle = \frac{3}{2} r_0 \left[\frac{R}{r_0} + \frac{\pi}{3\sqrt{3}} + \frac{1}{3} \ln \left(\frac{1 - \sqrt{\frac{R}{r_0}} + \frac{R}{r_0}}{\left(1 + \sqrt{\frac{R}{r_0}}\right)^2} \right) - \frac{2}{\sqrt{3}} \arctan \left[\frac{2\sqrt{\frac{R}{r_0}} - 1}{\sqrt{3}} \right] \right] / \ln \left(1 + \left(\frac{R}{r_0}\right)^{\frac{3}{2}} \right). \quad (25)$$

We can get the shape parameter r_0 numerically by inverting $\langle R \rangle$, which can be then used to define the Moore density parameter, ρ_0 , with the observed mass, M , contained within the radius, R , by inverting Eq. (23):

$$\rho_0 = \frac{3M}{8\pi r_0^3 \ln \left(1 + \left(\frac{R}{r_0}\right)^{\frac{3}{2}} \right)}. \quad (26)$$

Thus, the kinetic energy density is defined to be

$$\rho_K = \frac{1}{2} \frac{3}{V} \int \rho \sigma_v^2 dV = \frac{9}{2} \frac{\rho_0 r_0^3}{R^3} \int_0^R \frac{r^{\frac{1}{2}}}{r^{\frac{3}{2}} + r_0^{\frac{3}{2}}} \sigma_v^2 dr. \quad (27)$$

Assuming a constant average velocity dispersion, it reads

$$\rho_K = \frac{1}{2} \frac{M}{V} 3\sigma_v^2 = 3\rho_0 \left(\frac{r_0}{R}\right)^3 \ln \left(1 + \left(\frac{R}{r_0}\right)^{\frac{3}{2}} \right) \sigma_v^2 = \frac{9}{8\pi} \frac{M}{R^3} \sigma_v^2, \quad (28)$$

still as in Ref. [11].

The potential energy is given by

$$\begin{aligned} \rho_W &= -\frac{4\pi}{4\pi R^3/3} \int_0^R \frac{\rho(r)GM(r)}{r} r^2 dr = -\frac{8\pi Gr_0^5 \rho_0^2}{R^3} \int_0^{\frac{R}{r_0}} \frac{\ln(1 + X^{\frac{3}{2}})}{X^{\frac{1}{2}}(1 + X^{\frac{3}{2}})} dX \\ &= -\frac{8\pi Gr_0^5 \rho_0^2}{R^3} F\left(\frac{R}{r_0}\right). \end{aligned} \quad (29)$$

Taking the ratio of Eqs. (28) and (29) we find:

$$\frac{\rho_K}{\rho_W} = -\frac{r_0}{GM} \frac{\ln^2 \left(1 + \left(\frac{R}{r_0}\right)^{\frac{3}{2}} \right)}{F\left(\frac{R}{r_0}\right)} \sigma_v^2 \quad (30)$$

Table 1 Velocity dispersions from the various observations of A586 as given by Ref. [12].

Method	σ (Km/s)
X-ray Luminosity	1015 ± 500
X-ray Temperature	1174 ± 130
Weak lensing	1243 ± 58
Velocity distribution	1161 ± 196

2.4 Einasto's profile

The Einasto density profile [24–26] was originally used to describe the internal density profiles of galaxies and has been proposed as a better fit model for Λ CDM haloes [31–33]:

$$\rho = \rho_e \exp \left[-d_n \left(\left(\frac{r}{r_e} \right)^{\frac{1}{n}} - 1 \right) \right] = \rho_0 \exp \left[-2n \left(\frac{r}{r_{-2}} \right)^{\frac{1}{n}} \right], \quad (31)$$

where $\rho_0 = \rho_e e^{d_n}$ is the central density and r_{-2} the radius at which the slope $d \ln \rho / d \ln r = -2$, the isothermal value. The radius r_e is defined such that it contains half the total mass and d_n is an integration boundary to ensure that. n gives the strength of the density fall. From Eq. (31) the corresponding mass then reads:

$$M = 4\pi \int_0^R \rho_0 \exp \left[-2n \left(\frac{r}{r_{-2}} \right)^{\frac{1}{n}} \right] r^2 dr. \quad (32)$$

The mean radius $\langle R \rangle$ then becomes defined with

$$M \langle R \rangle = 4\pi \int_0^R \rho_0 \exp \left[-2n \left(\frac{r}{r_{-2}} \right)^{\frac{1}{n}} \right] r^3 dr. \quad (33)$$

We can get the shape parameter r_{-2} from observing the mean intergalactic distance and numerically solving Eq. (33) together with Eq. (32).

We can then use it to compute the central density parameter ρ_0 by making use of Eq. (32). The kinetic and potential energy densities are computed from their definition

$$\rho_K = \frac{1}{2} \frac{3}{V} \int \rho \sigma_v^2 dV \rho_W, \quad \rho_W = -\frac{4\pi}{4\pi R^3/3} \int_0^R \frac{\rho(r)GM(r)}{r} r^2 dr, \quad (34)$$

through numerical integration. Note that it is also possible to perform the integrations analytically as done for the previous cases and find expressions relating the profile parameters and the virial ratio to the data M , $\langle R \rangle$ and σ . However, since these expressions for the Einasto profile are not particularly illuminating we will omit them.

Table 2 Virial ratio from the various observations of A586 obtained from data of Ref. [12] using different density profiles.

Method	Top Hat	NFW	Isothermal
X-ray Luminosity	-0.516 ± 0.516	-0.408 ± 0.407	-0.353 ± 0.352
X-ray Temperature	-0.691 ± 0.190	-0.545 ± 0.150	-0.472 ± 0.130
Weak lensing	-0.774 ± 0.145	-0.611 ± 0.115	-0.529 ± 0.099
Velocity distribution	-0.676 ± 0.253	-0.533 ± 0.200	-0.461 ± 0.173
Moore	Einasto $n = 1$	Einasto $n = 6$	
-0.316 ± 0.315	-0.416 ± 0.415	-0.405 ± 0.404	
-0.423 ± 0.116	-0.556 ± 0.153	-0.542 ± 0.149	
-0.474 ± 0.089	-0.624 ± 0.117	-0.608 ± 0.114	
-0.413 ± 0.155	-0.544 ± 0.204	-0.530 ± 0.199	

3 Analysis of A586 cluster

3.1 Data Analysis

In the analysis of A586 we used the same data used in the original analysis performed in [11], that is:

- member galaxy coordinates
- total mass inside a radius R , obtained from weak lensing measurements [12]:

$$M = (4.3 \pm 0.7) \times 10^{14} M_{\odot} \quad R = 422 \text{ Kpc} \quad (35)$$

- velocity dispersion from different sources, table 1.

Using the coordinates of the galaxies that compose A586 we can compute the average distance between a galaxy and the centre of the cluster, $\langle R \rangle$. We start by determining the centre of the cluster. This is done by computing the average declination and right ascension from the coordinates of the 31 galaxies in the cluster.

The distance of a galaxy i , with coordinates (α_i, δ_i) , to the centre of the cluster (α_c, δ_c) is given by:

$$r_i^2 = 2d^2[1 - \cos(\alpha_i - \alpha_c)\cos(\delta_c)\cos(\delta_i) - \sin(\delta_c)\sin(\delta_i)]. \quad (36)$$

Using Eq. (36) to compute r_i for all galaxies in the reduced sample and then taking the average:

$$\langle R \rangle = 223.6 \text{ Kpc}. \quad (37)$$

We can then proceed to compute the shape parameters of the various density profiles as described in the previous section and through them compute the virial ratio and the interaction between DE and DM.

Table 3 Summary of A1689 available data

Parameter	Value	Reference
ρ_0 ($10^{-25}h^2gr/cm^3$)	9.6 ± 1.8	[28]
r_0 ($h^{-1}kpc$)	175 ± 18	[28]
kT_x (KeV)	$9.2^{+0.4}_{-0.3}$	[27]
σ_{dyn} (Km/s)	1172^{+123}_{-99}	[29]
R_{dyn} ($h^{-1}Mpc$)	2.26	[29]

Table 4 NFW fit to A1689 lensing data.

Parameter	Value	Error
ρ_0 ($10^{-25}h^2gr/cm^3$)	4.513	0.330
r_0 ($h^{-1}kpc$)	271.6	12.5
\mathcal{R}^2	0.999	–

3.2 Comments on the results for A586

We present our results in table 2. One sees that the analysis of this cluster with a top hat profile is in agreement with the findings of Ref. [11]. We observe consistently that using weak lensing velocity dispersion (as performed in Ref. [11]) yields a higher virial ratio. We stress that the weak lensing velocity dispersion is not the most adequate data source as it introduces correlations between mass and velocity estimation. It is crucial to avoid these correlations as the aim of this work is to detect deviations to the virial equilibrium and interpret these as an effect due to DE-DM interaction.

4 Analysis of the A1689 cluster

In table 3 we gather the data available for A1689. As already mentioned, for this cluster we find the density and shape parameters for the different profiles by directly fitting them to the 2D surface density obtained from weak and strong lensing. The relation between the 2D surface density $\kappa(R)$ and the total 3 dimensional mass density $\rho(r)$ is given by

$$\kappa(R) = \frac{2}{\Sigma_{crit}} \int_R^\infty \frac{\rho(r)rdr}{\sqrt{r^2 - R^2}}, \quad (38)$$

where Σ_{crit} is the critical density for lensing, which depends on the background cosmology and also on the lens and source sample. For the data we are considering, $\Sigma_{crit} = 1.0122 h g/cm^2$ [28], for $H_0 = 100h km/s/Mpc$ and observationally $h \simeq 0.7$. Then, by letting $\rho(r)$ be NFW, isothermal sphere, Moore, or Einasto, we estimate the parameters of these four density profiles.

In the ensuing analysis, we will consider two methods for estimating velocity dispersion: galaxy dynamics and X-ray temperature, as shown in table 3. While the velocity dispersion from the galaxy dynamics is a direct measurement, converting the X-ray temperature into a velocity dispersion involves assumptions that must be explained. Defining $\beta = \sigma_v^2(kT/\mu m_p)^{-1}$, where μ

Table 5 Moore fit to A1689 lensing data.

Parameter	Value	Error
ρ_0 ($10^{-25}h^2gr/cm^3$)	1.064	0.525
r_0 ($h^{-1}kpc$)	357	102
\mathcal{R}^2	0.973	-

Table 6 Einasto fit to A1689 lensing data.

Parameter	$n = 1$		$n = 6$	
	Value	Error	Value	Error
ρ_0 ($10^{-25}h^2gr/cm^3$)	46.49	5.165	66005	7358
r_0 ($h^{-1}kpc$)	122.5	8.47	467.3	31.99
\mathcal{R}^2	0.9834	-	0.998	-

and m_p are the reduced nuclear mass and the proton mass, allows for computing σ_v knowing kT once β is specified. To first approximation one can assume the hypothesis of density energy equipartition, which corresponds to setting $\beta = 1$. For this choice we find $\sigma_v = (1232 \pm 27) km/s$. Other values for β might be used, in particular see e.g. Ref. [29]. Another issue related to the velocity dispersion is the region in which it is measured. In the case of σ_v coming from galaxy dynamics, the measurements are taken in a spherical region whose radius is the distance to the centre of the outermost galaxy. For the current cluster, this is found to be $2.26h^{-1}Mpc$. In the case of X-ray temperature measurements, these are taken up to a radius r_{2500} , i.e. the radius at which the local density is 2500 times the critical density around the redshift of the cluster. Assuming the Λ CDM cosmology, we find this to be of order $300h^{-1}kpc$. Notice that the exact value of r_{2500} depends on the density profile as it is assumed, nonetheless there is an order of magnitude difference relative to R_{dyn} .

4.1 NFW profile

In Ref. [28] a joint X-ray and lensing analysis is performed and the data has been fitted to an NFW profile, the results of which are displayed in table 3. Nonetheless we perform our own fit to the lensing data, the results of which are shown in table 4.

Since the method used for computing ρ_K/ρ_W for A1689 is slightly different from the one used for A586, the value and error of the ratio will now be given in terms of the fitted parameters ρ_0 and r_0 instead of M and $\langle R \rangle$. The kinetic to potential energy density ratio is now given by

$$\frac{\rho_K}{\rho_W} = -\frac{3\sigma_v^2}{8\pi G\rho_0 r_0^2} \frac{\left[\left(1 + \frac{R}{r_0}\right) \ln \left(1 + \frac{R}{r_0}\right) - \frac{R}{r_0} \right] \left(1 + \frac{R}{r_0}\right)}{\left[\left(1 + \frac{R}{r_0}\right) \left\{ \frac{1}{2} \left(1 + \frac{R}{r_0}\right) - \ln \left(1 + \frac{R}{r_0}\right) \right\} - \frac{1}{2} \right]}, \quad (39)$$

and the error is found by applying Eq. (11) to the previous equation.

Table 7 Virial ratio from the various observations of A1689 given by Refs. [28,27,29].

Method	NFW	NFW [28]	Isothermal
X-ray Temperature	-0.518 ± 0.060	-0.538 ± 0.144	-0.715 ± 0.067
Velocity distribution	-0.408 ± 0.099	-0.485 ± 0.173	-0.647 ± 0.146
	Moore	Einasto $n = 1$	Einasto $n = 6$
	-0.549 ± 0.391	-0.527 ± 0.093	-0.520 ± 0.086
	-0.479 ± 0.389	-0.473 ± 0.130	-0.353 ± 0.098

For completeness we compute the ratio ρ_K/ρ_W using our best fit and the fit found in Ref. [28]. The results are displayed in table 7.

4.2 Isothermal sphere density profile

Following the procedure described above, we fit the projected mass data obtained from lensing measurements to the isothermal mass profile given by Eq. (12). One should notice that the isothermal profile, unlike the NFW, Moore and Einasto profiles, has only one free parameter, namely $\rho_0 r_0^2$. The fit to the data yields $\rho_0 r_0^2 = (3.987 \pm 0.333) \times 10^{-21}$ with $\mathcal{R}^2 = 0.845$. As indicated by the low value of \mathcal{R}^2 the isothermal profile is not very suitable to describe the mass distribution in the cluster A1689. This can also be seen in Figure 1. The energy density ratio is given in terms of the fitted parameter and the velocity dispersion by:

$$\frac{\rho_K}{\rho_W} = -\frac{3}{8\pi} \frac{\sigma_v^2}{Gr_0^2 \rho_0}, \quad (40)$$

with an error given by Eq. (11). Note that Eq. (40) is independent of the region where the velocity dispersion is measured, R . This is a characteristic feature of this profile. In Table 7 we display the results found by applying the isothermal profile to the study of A1689.

4.3 Moore's profile

Repeating the above procedure for the Moore's profile with data depicted in Table 5 we get the results shown in Table 7 from which we can see that no signal of DE-DM interaction can be seen as no deviation from the virial ratio value $-1/2$ is unambiguously seen.

4.4 Einasto's profile

Repeating the above procedure for the Einasto profile with data depicted in Table 6 we obtain the results shown in Table 7.

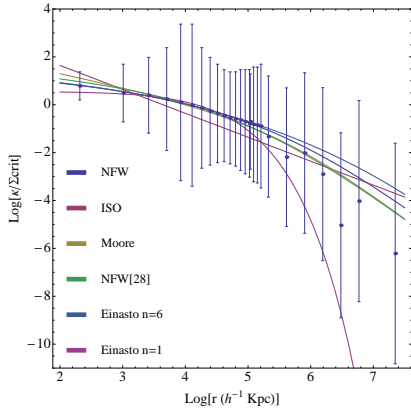


Fig. 1 Fits to 2D surface density for A1689.

5 DE-DM Interaction

In this section we relate the virial ratios computed above to the interaction parameter between DM and DE following Ref. [11]. We start by briefly reviewing how the interaction is parametrised and how this parameter is related to the virial ratio in relaxed structures. In Ref. [11] the interaction was analysed within the context of two distinct models of interacting DE: coupled quintessence [7] and the generalized Chaplygin Gas (GCG) [9]. It was shown that for $\omega_{DE} = -1$, the coupling parameter of the interacting quintessence, ξ (cf. below), is related to the α parameter of the GCG equation of state $p = -A/\rho^\alpha$, by the scaling parameter (defined below) $\eta = 3(1 + \alpha)$. Keeping this mapping between the two distinct models in mind, we review how to relate virial ratio the interaction parameter in the context of the coupled quintessence model.

The conservation equations for DM and DE read

$$\dot{\rho}_{DM} + 3H\rho_{DM} = \xi H\rho_{DM}, \quad (41)$$

$$\dot{\rho}_{DE} + 3H\rho_{DE}(1 + \omega_{DE}) = -\xi H\rho_{DM}. \quad (42)$$

It is assumed that there is a scaling behavior between the DE and DM energy densities,

$$\frac{\rho_{DE}}{\rho_{DM}} = \frac{\Omega_{DE}}{\Omega_{DM}} a^\eta, \quad (43)$$

where η describes the scaling and is related to the coupling ξ by [11]

$$\xi = -\frac{\eta + 3\omega_{DE}}{1 + (\Omega_{DM0}/\Omega_{DE0})a^{-\eta}}. \quad (44)$$

Following the derivation of the Layzer-Irvine equation in Ref. [34], noting that the scaling of the matter kinetic energy with the scale factor is unchanged

by the presence of interaction with DE, $\rho_K \propto a^{-2}$, and that the interaction will modify the scaling of the potential energy with a to $\rho_W \propto a^{\xi-1}$ one finds [11]

$$\dot{\rho}_{DM} + H(2\rho_K + \rho_W) = \xi\rho_W H. \quad (45)$$

This is the modified Layzer-Irvine equation. Assuming that locally $\dot{\rho} \approx 0$, we find that the virial theorem is modified to

$$\frac{\rho_K}{\rho_W} = -\frac{1}{2} + \frac{\xi}{2}, \quad (46)$$

where ξ is the interaction strength as defined in Eqs. (41) and (42).

We are therefore mapping deviations from virial equilibrium to the existence of DE-DM interaction. If the data on a particular cluster yields $\rho_K/\rho_W > -1/2 \Rightarrow \xi > 0$ and the energy transfer occurs from DE to DM. Conversely $\rho_K/\rho_W < -1/2 \Rightarrow \xi < 0$ and the energy transfer occurs from DM to DE.

As already stressed in the previous section, the results in tables 2 and 7 do not point to a preferred direction of the deviation of the ratio from its canonical value of $1/2$. Therefore there is no preferred sign for ξ and the results are largely consistent with $\xi = 0$. This contrasts with the results found in [11, 13] where the analysis of the A586 cluster with a top hat profile and weak lensing inferred velocity dispersion pointed towards $\xi < 0$. In fact, this suggests that changing the density profile and considering the related methodological difficulties do not allow for a definite conclusion on the virial ratio. We believe that the current analysis represents a step forward relative to the original proposal as it deals with more realistic density profiles and uses uncorrelated data sources in the estimation of the velocity dispersion. However, in order to distinguish between the different physical scenarios $\xi > 0$, $\xi < 0$ and $\xi = 0$ it is crucial to have a better understanding both of the mass distribution within the clusters and a more importantly a more accurate knowledge of their dynamical state. This will allow to decrease the error bars and detect putative deviations of the ratio from -0.5 .

6 Conclusions

In this work we have analyzed the virial equilibrium of clusters A586 and A1689 using four density profiles, namely NFW, isothermal spheres and Moore's and Einasto's profiles. The method employed represents an evolution from the original proposal as it deals with more realistic mass distributions. For the A586 cluster we have only found evidence of deviation of the virial ratio $\rho_K/\rho_W = -1/2$ for the over-simplistic Top-Hat density profile, in accordance with [11]. In what concerns cluster A1689, we have not encountered a convincing evidence of this interaction except when using the uni-parametric isothermal sphere distribution. This could reflect the claims on A1689 that it is not a relaxed cluster, in particular, that it exhibits signs of triaxiality [36]. Despite the fact that search for interaction with more realistic mass profiles has not returned a clear signal in either cluster, one should stress that the

encountered error bars are still too large at present. In order to study the interaction between DE and DM via deviations from the virial equilibrium it is crucial to have a better understanding of the cluster mass distribution and of their dynamical state. We believe N-body simulations have a crucial role to play in this problem.

Acknowledgments

The authors would like to thank Felipe Andrade Santos for discussions on the A1689 X-ray substructure, and Doron Lemze, Keiichi Umetsu and Adi Zitrin for several discussions and for kindly allowing us to use their data of cluster A1689. The work of O.B. is partially supported by the Fundação para a Ciência e a Tecnologia (FCT) project PTDC/FIS/111362/2009. The work of F.G.P. is supported by the FCT grant SFRH/BD/35756/2007. The work of M.L.D. is supported by CSIC (Spain) under the contract JAEDoc072, with partial support from CICYT project FPA2006-05807, at the IFT, Universidad Autonoma de Madrid, Spain.

References

1. A. E. Bernardini and O. Bertolami, Phys. Lett. B **662** (2008) 97 [arXiv:0802.4449 [hep-ph]]. A. E. Bernardini and O. Bertolami, Phys. Rev. D **77** (2008) 085032 [arXiv:0802.2199 [hep-ph]].
2. V. Silveira and A. Zee, Phys. Lett. B **161** (1985) 136.
3. M. C. Bento, O. Bertolami, R. Rosenfeld and L. Teodoro, Phys. Rev. D **62** (2000) 041302 [arXiv:astro-ph/0003350]. M. C. Bento, O. Bertolami and R. Rosenfeld, Phys. Lett. B **518** (2001) 276 [arXiv:hep-ph/0103340].
4. M. C. Bento and O. Bertolami, Phys. Lett. B **675** (2009) 231 [arXiv:0901.1818 [astro-ph]].
5. M. C. Bento, A. E. Bernardini and O. Bertolami, J. Phys. Conf. Ser. **174** (2009) 012060 [arXiv:0904.1933 [hep-ph]].
6. T. Barreiro, O. Bertolami and P. Torres, to appear in Mon. Not. R. Astron. Soc. arXiv:1004.4562 [astro-ph.CO].
7. L. Amendola, Phys. Rev. D **62** (2000) 043511 [arXiv:astro-ph/9908023].
8. A. Y. Kamenshchik, U. Moschella and V. Pasquier, Phys. Lett. B **511**, 265 (2001) [arXiv:gr-qc/0103004]; N. Bilic, G. B. Tupper and R. D. Viollier, Phys. Lett. B **535**, 17 (2002) [arXiv:astro-ph/0111325].
9. M. C. Bento, O. Bertolami and A. A. Sen, Phys. Rev. D **66** (2002) 043507 [arXiv:gr-qc/0202064].
10. O. Bertolami and R. Rosenfeld, Int. J. Mod. Phys. A **23** (2008) 4817 [arXiv:0708.1784 [hep-ph]].
11. O. Bertolami, F. Gil Pedro and M. Le Delliou, Phys. Lett. B **654** (2007) 165 [arXiv:astro-ph/0703462].
12. E. Cypriano, G. Neto, L. Sodre and J. Kneib, Astrophys. J. **630** (2005) 38.
13. O. Bertolami, F. G. Pedro and M. Le Delliou, Gen. Rel. Grav. **41**, 2839 (2009) [arXiv:0705.3118 [astro-ph]].
14. E. Abdalla, L.R.W. Abramo, L. Sodre, Jr., B. Wang, Phys. Lett. B **673**, 107 (2009); E. Abdalla, L.R.W. Abramo, J.C.C. de Souza, Phys. Rev. D **82**, 023508 (2010) .

15. T. F. Laganá, G. B. Lima Neto, F. Andrade-Santos and E. S. Cypriano, *Astron. & Astrophys.* **485**, 633 (2008)
16. J. F. Navarro, C. S. Frenk and S. D. M. White, *Astrophys. J.* **462**, 563 (1996) [arXiv:astro-ph/9508025].
17. R. B. Larson, *Mon. Not. R. Astron. Soc.* **145**, 271 (1969).
18. M. V. Penston, *Mon. Not. R. Astron. Soc.* **144**, 425 (1969).
19. J. E. Gunn and J. R. Gott, *Astrophys. J.* **176**, 1 (1972).
20. J. A. Fillmore and P. Goldreich, *Astrophys. J.* **281**, 1 (1984).
21. E. Bertschinger, *Astrophys. J. Suppl.* **58**, 39 (1985).
22. P. J. E. Peeble, *The Large Scale Structure of the Universe* (Princeton, NJ: Princeton University Press, 1980).
23. B. Moore, T. Quinn, F. Governato, J. Stadel, and G. Lake, *Mon. Not. R. Astron. Soc.*, **310**, 1147 (1999).
24. J. Einasto, *Trudy Inst. Astrofiz. Alma-Ata*, **5**, 87 (1965).
25. J. Einasto, *Tartu Astron. Obs. Publ.*, **36(5-6)**, 414 (1968).
26. J. Einasto, *Astrofizika*, **5**, 137 (1969).
27. H. Hoekstra, *Mon. Not. Roy. Astron. Soc.* **379**, 317 (2007) [arXiv:0705.0358 [astro-ph]].
28. D. Lenze, R. Barkana, T. J. Broadhurst and Y. Rephaeli, arXiv:0711.3908 [astro-ph].
29. M. Girardi and M. Mezzetti, arXiv:astro-ph/0010302.
30. Y. P. Jing, and Y. Suto, *Astrophys. J. Lett.*, **529**, L69 (2000).
31. A. W. Graham, D. Merritt, B. Moore, J. Diemand and B. Terzic, *Astron. J.* **132** (2006) 2685 [arXiv:astro-ph/0509417].
32. A. W. Graham, D. Merritt, B. Moore, J. Diemand and B. Terzic, *Astron. J.* **132** (2006) 2701 [arXiv:astro-ph/0608613].
33. A. Lapi and A. Cavaliere, arXiv:1010.2602 [astro-ph.CO].
34. P. J. E. Peebles, *Principles of physical cosmology* (Princeton, N.J.:Princeton University Press,1993).
35. E. Komatsu *et al.*, arXiv:1001.4538 [astro-ph.CO].
36. M. Sereno, K. Umetsu, [arXiv:1105.4994 [astro-ph.CO]].